SCIENCE CHINA
Earth Sciences

•ARTICLE•

July 2023 Vol.66 No.7: 1521–1534
https://doi.org/10.1007/s11430-022-1117-x

The decadal abrupt change in the global land vapor pressure deficit

Mengqi CHENG[1], Zhiyan ZUO[1,3,4*], Zouxing LIN[1], Qinglong YOU[1] & Huan WANG[1,2]

[1] *Department of Atmospheric and Oceanic Sciences, Institute of Atmospheric Sciences, Fudan University, Shanghai 200438, China;*
[2] *The Faculty Geography Resource Sciences, Sichuan Normal University, Chengdu 610101, China;*
[3] *Shanghai Frontiers Science Center of Atmosphere-Ocean Interaction, Shanghai 200438, China;*
[4] *National Observations and Research Station for Wetland Ecosystems of the Yangtze Estuary, Shanghai 202183, China*

Received September 28, 2022; revised May 8, 2023; accepted May 19, 2023; published online June 13, 2023

Abstract The vapor pressure deficit (VPD) is an important variable used to characterize atmospheric aridity. This paper analyses the spatial and temporal characteristics of the decadal abrupt change (DAC) in the global land VPD after 1980 using monthly scale data from the Climatic Research Unit. The results show that 60.5% of the global land area underwent a significantly increased decadal abrupt change (IDAC) in the VPD, and the persistent IDAC of the VPD was obvious in the middle and low latitudes of Eurasia, Africa and parts of South America but not in central North America or Western Siberia. From 1980 to 2020, most regions experienced no more than two persistent IDACs, while more than two significant increases occurred mainly around the Mediterranean and in eastern South America. The persistent IDAC occurred relatively early in the middle and low latitudes of Eurasia, Africa, and eastern South America and after 2000 in the high latitude regions, Eastern Europe, and near the Qinghai-Tibet Plateau. The regions where the persistent IDAC lasted longer than 10 years mainly included North Africa, West Asia, eastern South America, and parts of East Asia, indicating that the persistent increases in atmospheric aridity in these regions were obvious. In general, the persistent IDAC that began in 1993–2000 was significantly more than that occurred in other periods and lasted longer than that before 1990, suggesting that the land area experiencing an abrupt increase has an expansion after the 1990s and that the role of water limitation in this persistent IDAC in Central Asia and most of China strengthened. In addition, the VPD showed another large-scale persistent IDAC over the global land region in 2009, indicating that global atmospheric aridity intensified over the last decade. At the same time, in a few global regions, the VPD has exhibited decreased decadal abrupt changes (DDACs) with durations shorter than 2 years.

Keywords Vapor pressure deficit, Atmospheric aridity, Decadal abrupt changes, Spatial and temporal characteristics

Citation: Cheng M, Zuo Z, Lin Z, You Q, Wang H. 2023. The decadal abrupt change in the global land vapor pressure deficit. Science China Earth Sciences, 66 (7): 1521–1534, https://doi.org/10.1007/s11430-022-1117-x

1. Introduction

The global surface temperature generally increases as the carbon dioxide (CO_2) concentration increases, and soil drought and atmospheric aridity are intensifying in most global areas; the degree of atmospheric aridity is directly related to the occurrence and development of forest fires, vegetation mortality and extreme events. For example, when the atmosphere is highly arid, forest fire occurrences increase significantly, vegetation mortality increases, and the intensity and frequency of compound dry-hot extreme events increase significantly (Williams et al., 2015; Novick et al., 2016; Zhou et al., 2019b; Yuan et al., 2019; Friedlingstein et al., 2022). Therefore, there has recently been a growing interest in atmospheric aridity changes in the research community, especially among policy-makers and scientists

* Corresponding author (E-mail: zuozhy@fudan.edu.cn)

(Zhou et al., 2019b; Yuan et al., 2019).

The vapor pressure deficit (VPD) is the difference between the saturated vapor pressure and the actual vapor pressure; this is an important variable commonly used to indicate atmospheric aridity and can reflect the atmospheric demand for water (Novick et al., 2016; Ficklin and Novick, 2017; Barkhordarian et al., 2021). A higher VPD corresponds to a drier atmosphere, and a lower VPD corresponds to a wetter atmosphere. In most parts of the world, when the VPD is too high, plant stomata tend to close to reduce water losses, resulting in reduced plant photosynthesis; this process partially offsets the increased carbon uptake caused by the CO_2 fertilization effect and poses a challenge for global greening alleviate the increased surface air temperature (Zeng et al., 2017; Zhou et al., 2019a; Piao et al., 2020; Grossiord et al., 2020; Song et al., 2022). However, it has also been suggested that photosynthesis is positively correlated with the VPD in the humid areas of the Amazon rainforest due to leaf turnover, radiation, etc. Although this positive correlation is weakened or reversed when the VPD is more extreme, the results show significant regional differences in the ecosystem productivity response to the VPD (Green et al., 2020). In addition, the VPD is strongly correlated with climate variables such as the temperature, evapotranspiration, and soil moisture (Zhou et al., 2019b; Barkhordarian et al., 2021). For example, abnormally high VPD is often accompanied by abnormally low soil moisture, and the frequency and intensity of compound extreme events comprising atmospheric aridity and soil drought are expected to increase further in the future, causing much greater impacts on ecosystem productivity than individual extreme events (Zhou et al., 2019b; Lu et al., 2022). At the same time, the VPD can also indirectly drive the growth rate of atmospheric CO_2 (Barkhordarian et al., 2021; He et al., 2022). It is evident that regional abnormal VPD and persistent abnormal changes impact the climate and ecosystem, so it is necessary to investigate the characteristics of long-term VPD changes in depth.

Under the background of global warming, a significant increase in the global average VPD occurred in the 1990s, and many studies have focused on the impact of this VPD increase on the vegetation ecology and climate (Yuan et al., 2019; Lu et al., 2022; He et al., 2022), but few studies have focused on the spatial or temporal characteristics of abrupt VPD changes themselves at the decadal scale. The decadal abrupt change (DAC) in the VPD can directly reflect the significant changes and regional differences in VPD at a relatively long time scale in the historical period and can also reflect the influencing factors of those significant changes in the VPD and the responses of other climate variables in this particular period, thus providing an important basis for exploring the formation and development mechanisms of atmospheric aridity and isolating the independent effect of the VPD from the impacts of other factors (Liu et al., 2020; Humphrey et al., 2021). How does the occurrence time of the increased decadal abrupt change (IDAC) of the VPD differ among different regions of the world? Do some differences in the duration of IDACs exist among different regions? Are there regions with decreased decadal abrupt changes (DDACs) in the VPD? To answer these questions, we used monthly scale data from the Climatic Research Unit (CRU) to analyse the spatial and temporal characteristics of the VPD DAC at the global land scale from 1980 to 2020 by the moving *t* test technique. The results reveal the changes in the VPD and the development of atmospheric aridity in detail and provide a reference for analysing the physical mechanisms associated with VPD changes and their impacts on the climate system and ecosystem, thereby improving the responses of models to atmospheric aridity, reducing the prediction uncertainty and solving the problems related to atmospheric aridity (Liu et al., 2020; Zhou et al., 2021; Berg and McColl, 2021; Humphrey et al., 2021; Liu et al., 2021).

2. Data and methods

2.1 Data

The study data were obtained from the monthly scale observation land dataset CRU_ts4.05 provided by the CRU (Harris et al., 2020). An existing study has shown that VPD data calculated at the monthly scale are credible (He et al., 2022). We used the maximum (minimum) surface air temperature and actual vapor pressure in the CRU dataset to calculate the VPD, and the data provided by CRU were uniformly bilinearly interpolated to a horizontal spatial resolution of 1°×1° to ensure a consistent resolution for subsequent related studies. Greenland and Antarctica were excluded from the global land area in our data.

The VPD is defined as the difference between the saturated vapor pressure and the actual vapor pressure (kPa), which is calculated from the temperature and water vapor pressure according to the following equation (Allen et al., 1998):

$$\mathrm{SVP_{max}}=0.6108\times\exp\left(\frac{17.27\times T_{\max}}{T_{\max}+237.3}\right), \tag{1}$$

$$\mathrm{SVP_{min}}=0.6108\times\exp\left(\frac{17.27\times T_{\min}}{T_{\min}+237.3}\right), \tag{2}$$

$$\mathrm{SVP}=\frac{\mathrm{SVP_{max}}+\mathrm{SVP_{min}}}{2}, \tag{3}$$

$$\mathrm{VPD}=\mathrm{SVP}-\mathrm{AVP}, \tag{4}$$

where, $T_{\max}$ ($T_{\min}$) is the monthly average daily maximum (minimum) temperature (°C). $\mathrm{SVP_{max}}$ ($\mathrm{SVP_{min}}$) is the saturated vapor pressure (kPa) at the corresponding maximum (minimum) temperature, as calculated according to the empirical formula, SVP is the monthly mean saturated vapor

pressure (kPa), and AVP is the actual vapor pressure (kPa) provided by CRU. Since the equation is nonlinear, the estimated saturated vapor pressure and the corresponding VPD are smaller when the monthly average temperature is used, so the monthly average saturated vapor pressure should be calculated as the average of the saturated vapor pressure corresponding to T_{max} and T_{min} (Allen et al., 1998).

2.2 Methods

2.2.1 Moving t test technique

The M-K test, piecewise linear regression, and moving *t* test are commonly used in abrupt change detection tasks and have been applied in past VPD studies (Toms and Lesperance, 2003; Yuan et al., 2019; Yuan et al., 2021). The moving *t* test technique is used in this study; this method detects abrupt changes in the mean by examining whether the difference between the means of two subsamples is significant (Fu and Wang, 1992; Wei, 2007). Compared to the single abrupt change of VPD obtained by the M-K test (Yuan et al., 2021), the results obtained by the moving *t* test can include multiple different significant changes in a long time series. In some regions with complex variation characteristics, the moving *t* test can show more accurate and detailed information about multiple abrupt changes of variables in terms of the duration, number, and spatiotemporal interval (Xiao and Li, 2007; Wang et al., 2018).

The method is described as follows:

First, set a certain moment as the reference point, and the two subsamples taken in the two subseries x_1 and x_2 before and after this point are expressed as n_1 and n_2, respectively. The means of the subsamples are x_{m1} and x_{m2}, and the subsample variances are s_1^2 and s_2^2. The degree of freedom is calculated as $v=n_1+n_2-2$. The sample length of the subsample is set to 10 years in this study, so $n_1=n_2=10$, and the degree of freedom is 18.

The *t* statistic is defined as follows:

$$t=\frac{x_{m2}-x_{m1}}{s\cdot\sqrt{\frac{1}{n_1}+\frac{1}{n_2}}}, \tag{5}$$

where

$$s=\sqrt{\frac{n_1s_1^2+n_2s_2^2}{n_1+n_2-2}}, \tag{6}$$

where, length of the subsamples before and after the reference point is determined, and then a strict significance test is performed. When the absolute value of the statistic is greater than the given critical value (a confidence level of 99%), a significant difference is assumed between the mean values of the two subsamples before and after the reference point, and the point is considered to represent an abrupt change point. Finally, the reference point is set by moving the window to calculate the time series continuously.

The moving *t* test reflects the abrupt change in the mean over time, and we examine the change in the mean at the decadal scale by setting the subsample length to 10 years. The obtained abrupt change point was called the decadal abrupt mean change, decadal abrupt change, or abrupt change for short, written as DAC in this paper (Fu and Wang, 1992; Xiao and Li, 2007). To clarify the research object, a period during which the statistic continuously exceeded the critical value was considered a persistent DAC (a period with continuous DACs); the first year of the persistent DAC was considered to be the starting year of that persistent DAC; and the timespan of the whole persistent DAC was considered the duration of that persistent DAC. It can be understood that the abrupt change point represents a significant change in the decadal mean between the periods before and after that year. A persistent DAC is a period with continuous abrupt change points, representing a period of continuous significant change during which the variable remains in a relatively intense state of change. A positive statistic indicates that the VPD value changes in a positive direction, suggesting a VPD increase, which is an increased decadal abrupt change, represented by IDAC. A negative statistic indicates that the VPD value changes in a negative direction, indicating a decreased VPD, which is a decreased decadal abrupt change, represented by DDAC. In this paper, the global average and grid data were detected by moving *t* test to compare the spatial and temporal characteristics of the persistent DACs of the global VPD.

2.2.2 Multiple linear regression method

Multiple linear regression is an analytical method used to study correlations among multiple variables. The role and influence of the independent variables are studied by analysing the quantitative statistical relationships between multiple independent variables and a dependent variable (Shi, 2009; Huang, 2016).

The multiple linear regression equation is expressed as follows:

$$Y=b_0+b_1X_1+b_2X_2+...+b_iX_i(i=1,2,...,m), \tag{7}$$

where, Y is the dependent variable, X_i is the independent variable, b_i is the regression coefficient of X_i, also known as the partial regression coefficient, indicating the degree of change in the dependent variable Y for each unit change in the independent variable X_i, and b_0 is the intercept.

The standardized partial regression coefficients can be obtained by standardizing the partial regression coefficients as follows:

$$B_i=b_i\frac{s_i}{s_y}(i=1,2,...,m), \tag{8}$$

where, s_i is the standard deviation of the independent variable X_i, s_y is the standard deviation of the dependent variable Y, and B_i indicates that the dependent variable Y will change

by B_i standard deviations for each additional standard deviation of the independent variable X_i. Since B_i is dimensionless, it can be used to directly compare the effects of different variables on the dependent variable.

In this study, the effects of the temperature (X_1) and actual vapor pressure (X_2) as independent variables on the dependent variable VPD (Y) were investigated by this method. This analysis was performed using data processing software, referenced to http://dx.doi.org/10.5065/D6WD3XH5.

3. Results and analysis

3.1 Characteristics of the global land VPD

The climatological mean VPD for 1901–2020 over global land is shown in Figure 1a. The overall spatial distribution of the VPD shows higher VPD in middle and low latitudes and lower VPD in high latitudes; large VPD differences can be seen among different latitudes. For example, in parts of Africa, the VPD reached 3.5 kPa; in India and Australia, it exceeded 2 kPa in most areas; and in the high latitudes of Eurasia, it was only approximately 0.2 kPa. The VPD mainly decreased with increasing latitudes in the middle and high latitude regions, and the VPD distribution at low latitudes was consistent with the vegetation cover types (He et al., 2022). Specifically, the VPD was lower in tropical rainforest areas near the equator (such as the Amazon region in South America and central Africa) and rapidly increased when transitioning to desert areas at higher latitudes (such as the desert regions in northern Africa and West Asia); the VPD was also significantly higher in the scrubland areas of Australia, southern Africa and southwestern North America than in areas with other vegetation cover types at the same latitude. The overall characteristics of the climatological mean VPD suggest a wetter atmosphere at high latitudes and a drier atmosphere at middle and low latitudes, especially in some desert and scrubland areas, such as northern African deserts, West Asia and Australia.

An overall upwards VPD trend over the past 120 years can be found in the evolution characteristics of the global average land VPD from 1901 to 2020, as shown in Figure 1b. Specifically, this period can be divided into the following three stages: during the first stage, from 1900 to 1940, the VPD rose slowly; the second stage, from 1941 to 1975, was a period of slow decline in the VPD; and the third stage, from 1976 to 2020, was a period of dramatic increase during which the VPD showed a significant increasing trend, especially over the most recent 30 years. In general, the global average VPD exhibited an increase-decrease-increase process, with some periods of this process showing more significant changes than others; thus, the VPD exhibits obvious abrupt change characteristics.

To further understand the abrupt change characteristics of the global-average land VPD, we detected the DAC of the VPD time series using a moving t test to understand this phenomenon of a rapid change in a short term (Figure 1b). Seven persistent DACs occurred from 1901 to 2020, as shown in the results. In the first stage, four significant persistent IDACs were identified (with DAC durations of 1919, 1921–1923, 1925–1926, and 1930–1935); in the second stage, only one persistent DDAC was found, from 1943 to 1949; in the third stage, two significant persistent IDACs were identified (with DAC durations of 1979 and 1994–2011). The persistent IDAC with the longest duration began in 1994 and lasted until 2011 (N was chosen to be 10 in the moving t test technique, so the last statistical period was 2011–2020, after which the analysis was stopped due to the lack of subsamples in the subseries; thus the latest starting year considered in this study was 2011). The number of persistent IDACs was much higher than the number of persistent DDACs overall, and except for the period starting in 1994 with a long duration, all other persistent DACs were limited within 6 years and occurred mainly before 1980. Therefore, in our subsequent research, we focus on persistent IDACs that began after 1980. The starting year of the persistent IDAC with the longest duration was chosen as the piecewise point; then, piecewise linear regression was performed on the annual average series at 1994. The trend after 1994 (0.0022 kPa yr^{-1}) was significantly higher than that before 1994 (0.0001 kPa yr^{-1}) and passed the 99% significance test, further confirming that the related analysis of the persistent DAC effectively reflected the significant VPD changes. The global average VPD increased rapidly after the 1990s, and has been in a persistent abrupt increase for a long time.

3.2 Spatial and temporal characteristics of the VPD IDAC

Significant regional differences were observed in the VPD IDAC results, and the results of the moving t test on each grid point on land after 1980 (Figure 2a) show a large range of two or more persistent IDACs in eastern South America, Africa, and the middle and low latitudes of Eurasia, especially in Western Europe and North Africa, where the numbers of persistent IDACs were significantly higher than in other regions. In many areas of the globe, such as Western Siberia, central North America, Australia, and most of western South America, no VPD IDACs were identified. These results suggest that the atmospheric aridity in the middle and low latitudes has changed dramatically, while the changes in high latitude regions have been relatively moderate. In general, the areas with multiple persistent IDACs were found to concentrated mainly around the Mediterranean and in eastern South America, indicating a strong degree of atmospheric aridification in these areas that is deserving of

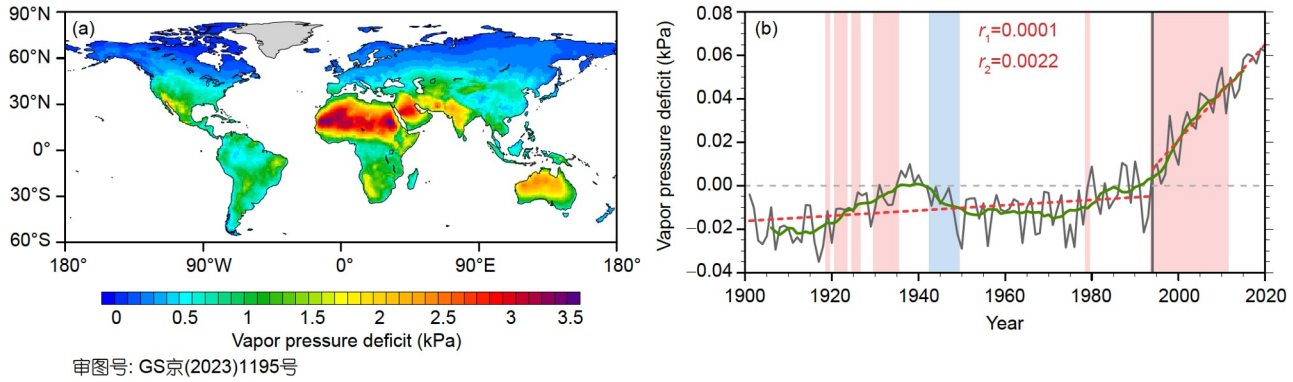

Figure 1 The spatial distribution of the climatological mean (a) and temporal evolution characteristics (b) of the global land VPD from 1901 to 2020. In panel (b), the black solid line is the global land average time series of the annual average monthly VPD anomalies, the red dotted lines are the trends of the VPD anomalies in the two periods before and after 1994, the green solid line is the 11-year running mean of the global average VPD anomalies, the red shadow is the persistent IDAC, the blue shadow is the persistent DDAC, and r_1 and r_2 are the regression coefficients (kPa yr^{-1}) for the two periods before and after 1994, respectively.

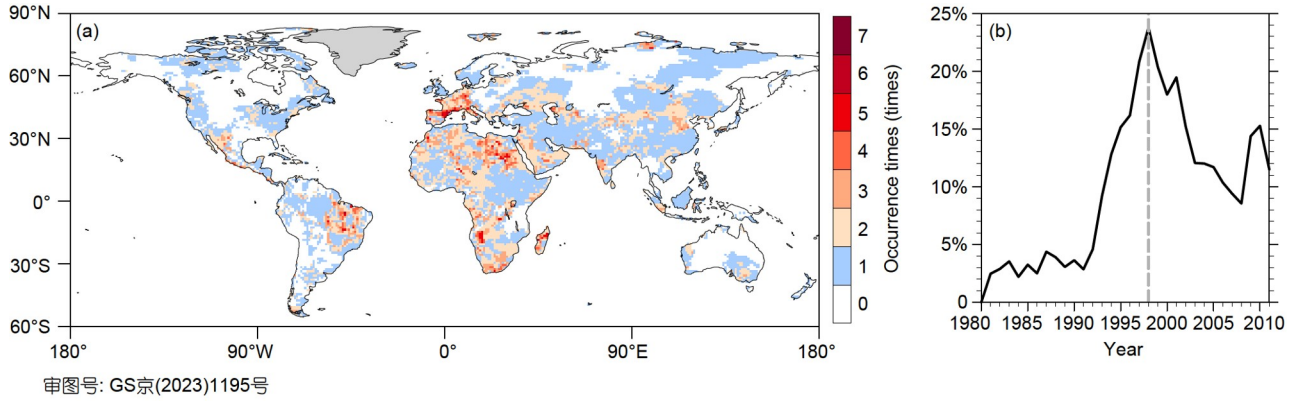

Figure 2 The spatial distribution of the number of the persistent IDAC occurrences (a) and the percentage of global land areas undergoing an IDAC (b) during 1980–2020. The percentages in panel (b) were calculated as the ratio of the land area in a state of IDAC to the total effective global land area; the total effective global land area refers to the global land area excluding Greenland and Antarctica.

further attention.

The grid points simultaneously in the abrupt increase state were counted to analyse the large-scale IDACs in space in different periods. Figure 2b shows the percentage of areas that experienced an IDAC in the corresponding year among the global effective land area. Four stages can be clearly seen in spatial IDAC range results. The figure shows that before 1991, the global regions that were experiencing abrupt VPD increases at the same time remained below 5%, a relatively small and stable percentage; beginning in 1992, this area increased rapidly, and the percentage was maximized in 1998, when 23.8% of the global land area was in a state of simultaneous abrupt increase; subsequently, from 1999 to 2008, the area began to decrease gradually, falling below 10% in 2008; and after 2009, another obvious range expansion that reached 14.4% occurred. In general, there were two significant areal expansions in the mid-late 1990s and approximately 2010, and the global expansion of this abrupt increase area indicated that the VPD was in a state of rapid increase in more increasing regions. This finding also indicates that the global land area has experienced a large-scale rapid VPD increase along with increased atmospheric aridity over the past decade.

We further quantified the DAC information and counted the appearance times of the persistent IDAC on all grid points (Figure 3a). The results show that 39.5% of the regions experienced no persistent IDACs; this category accounted for the highest proportion and corresponded mainly to high latitudes; 54.2% of the regions experienced one or two persistent IDACs, comprising more than half of the total study area, of which 37.5% had one occurrence and 16.8% had two occurrences; regions with three or more occurrences were fewer and relatively concentrated, accounting for only 6.3%; the percentage of regions with five or more occurrences was below 0.5%, and the maximum number of persistent IDACs experienced in a region was seven, but only 0.02% of the land areas experienced seven persistent IDACs, most of which were concentrated in parts of western Europe. The overall characteristics of the persistent IDAC occurrence times showed an areal decrease with an increasing occur-

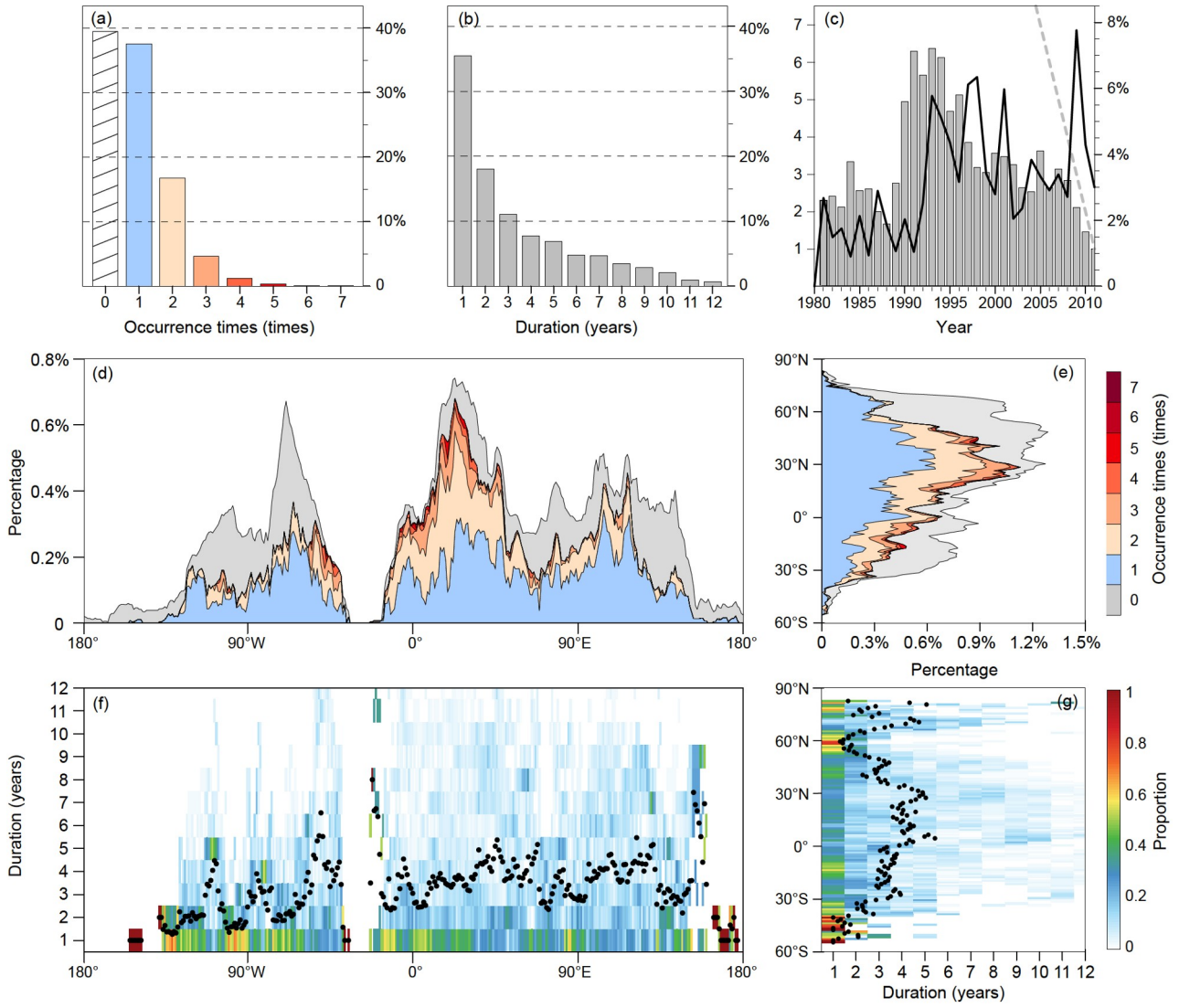

Figure 3 Statistical information of persistent IDACs that occurred on global lands from 1980 to 2020. (a) The percentages of the study area where different numbers of persistent IDACs occurred; (b) the distribution of persistent IDAC durations; (c) the starting year and average duration of all persistent IDACs; (d) and (e) the distribution of areas with different persistent IDAC occurrence times at each longitude and latitude, respectively; and (f) and (g) the proportion of different durations of persistent IDACs at each longitude and latitude, respectively. In panel (c), the histogram shows the average duration of all persistent IDACs in which the starting year is the stated year (year), the black solid line is the probability distribution that the starting year is that year in all persistent IDACs, and the grey dotted line is the fitted straight line for the time remaining to 2011. In panels (d) and (e), the percentage of areas with different persistent IDAC occurrence times at the given longitude (latitude) is indicated as the ratio of the area with different occurrence times at that longitude (latitude) to the total effective global land area, the single colour indicates the percentage of areas where this type persistent IDAC occurrence times, the grey area shows the percentage of regions without persistent IDACs, and the cumulative percentage of all types indicates the percentage of the total area of this longitude (latitude) range in the global land area. In panels (f) and (g), the proportion of each duration type at a given longitude (latitude) is indicated as the ratio of the number of persistent IDACs of this duration at this longitude (latitude) to the number of all persistent IDACs at this longitude (latitude), and the black point is the average duration at each longitude (latitude).

rence number, indicating that the phenomenon of multiple persistent IDAC occurrences may have been caused by the unique climate conditions in some regions. In addition, great differences in the distribution of persistent IDACs were observed among different longitudes (latitudes) (Figure 3d, 3e). In terms of the longitude, the areas that experienced persistent IDACs between 0 and 45°E were significantly larger than those in other longitude ranges, and only a small portion of the areas in each longitude range experienced no persistent IDACs; in addition, the area and proportion of areas with two or more persistent IDACs in this longitude range were also significantly higher than those in other longitude ranges. In terms of the latitude, relatively few areas had persistent IDACs north of 60°N, essentially only one persistent IDAC occurred in this range; while areas with persistent IDACs between 15°N and 45°N were more numerous, and the proportion reached the maximum near 30°N, and the proportion of areas with persistent IDACs was sig-

nificantly higher in this latitude range than in other ranges. The latitudinal area and proportion of areas with persistent IDACs in the total latitudinal area gradually decreased as the latitude transitioned southward from 30°N.

The duration distribution of all persistent IDACs is given in Figure 3b; from the figure, it can be seen that the longer the duration was, the lower the probability of occurrence was. More than half of the durations were 1–2 years (53.5%), meaning that IDACs in a large part of the world were observed mainly in 1 or 2 years, after which the VPD maintained a relatively stable change and no sustained intensification in atmospheric aridity occurred. However, 0.3% of all persistent IDACs exhibited durations exceeding 15 years, indicating that the aridification of the atmosphere in these regions has been increasing and that atmospheric conditions with intensifying aridity may cause severe damage to the local climate and ecosystem, requiring a focus on monitoring, detecting and conducting some targeted mitigation and adaptation studies. The distribution of the persistent IDAC durations only shorter than or equal to 12 years is shown in the figure due to the small proportion of durations longer than 12 years (1.9%). Further analysis of the proportions of different durations and the average duration of all persistent IDACs at each longitude (latitude) (Figure 3f, 3g) shows that the largest duration proportion was 1–2 years at most longitudes (latitudes); this proportion could exceed 80% at most longitudes (latitudes) with relatively few significant change areas. With regards to longitude, no obvious characteristic of the average duration was observed, with most durations ranging from 2 to 5 years. Among the latitude ranges, the average durations north of 50°N and south of 30°S were basically concentrated in 1 or 2 years, but longer durations accounted for a relatively large proportion near 70°N, where the average duration could reach 5 years. For the 0–30°N range, the proportion of the persistent IDAC durations longer than 2 years increased and the average duration increased to 4–6 years.

Analysing the starting year and average duration of persistent IDACs starting in the corresponding year (Figure 3c) revealed significant increases in both terms in the 1990s. Specifically, from the probability density distribution of the starting year, no significant characteristics were exhibited before 1992, when the distribution fluctuated at approximately 2%; the persistent IDAC that began in 1993–2001 accounted for a large proportion, and the occurrence probability during this period was roughly twice that before 1993, although large fluctuations still occurred; after that, the percentage decreased from 2002 to 2008; and the highest percentage of grid points (7.8%) was found in 2009, indicating that the persistent IDAC that began in 2009 was the most. In terms of the average duration, the average duration of persistent IDACs that began in 1981–1989 was relatively short, at approximately 2 years; the average duration from 1990 to 1997 was extended overall, especially in the early 1990s, when the duration increased rapidly compared to that before 1990 and exceeded 6 years in some years; the average duration decreased after 1998 and subsequently remained relatively stable at approximately 3 years. Notably, the decrease in the average duration during this later period does not indicate short-duration events but is more so the result of the moving *t* test method being halted after 2011 in Figure 3c. Overall, the prolonged duration during the early 1990s and the subsequent increase in persistent IDACs combined to cause a large portion of the global land area to be in a state of significant IDAC simultaneously in the 1990s, consistent with the findings shown in Figure 2b.

The starting years and durations of the first, second, and longest-duration persistent IDACs were compared at all grid points (Figure 4). Here, we considered that most of the information could be reflected by screening out these three times for comparison because only 6.3% of the study area experienced three or more persistent IDACs and the percentage of the third and subsequent persistent IDACs having the longest duration was only 3.2%. The starting year shows an overall distribution of early years in the middle and low latitude regions and late years in the high latitude regions. Specifically, in regions where only one persistent IDAC occurred, the first persistent IDAC in the middle and high latitudes of the Northern Hemisphere, north-western South America, and some other regions occurred after 2005, and a large portion of these events continued until 2011, when the moving *t* test stopped, while those in the middle and low latitudes generally occurred earlier, mostly before 2000. Regional differences in the starting year were observed in regions with multiple persistent IDACs. For example, persistent IDACs appeared in parts of Africa and Europe before 1990, while in Asia, they were concentrated mainly between 1993 and 2005. Among them, long timespans could be seen between the first and second persistent IDACs in the Middle East and northwest China, with the first appearing in approximately 1995 and the second appearing after 2005; these findings are consistent with the findings shown in Figure 3c. In terms of the event duration, most persistent IDACs with the longest duration were the first events, accounting for 82.7% of all the grid points in which IDACs occurred, and longer-duration events were concentrated in the middle and low latitudes, such as in eastern South America, Africa, the Middle East, and south-eastern China, where IDACs could last more than 10 years. On the whole, persistent IDACs began earlier and lasted longer in the middle and low latitudes, while they began relatively late in the high latitudes; these findings are consistent with the above conclusion that the persistent VPD IDACs occurred mainly in the mid-low latitudes in the 1990s and in the high latitudes after 2005 and that atmospheric aridity intensified first in the middle and low latitudes. It should be noted that some areas experienced

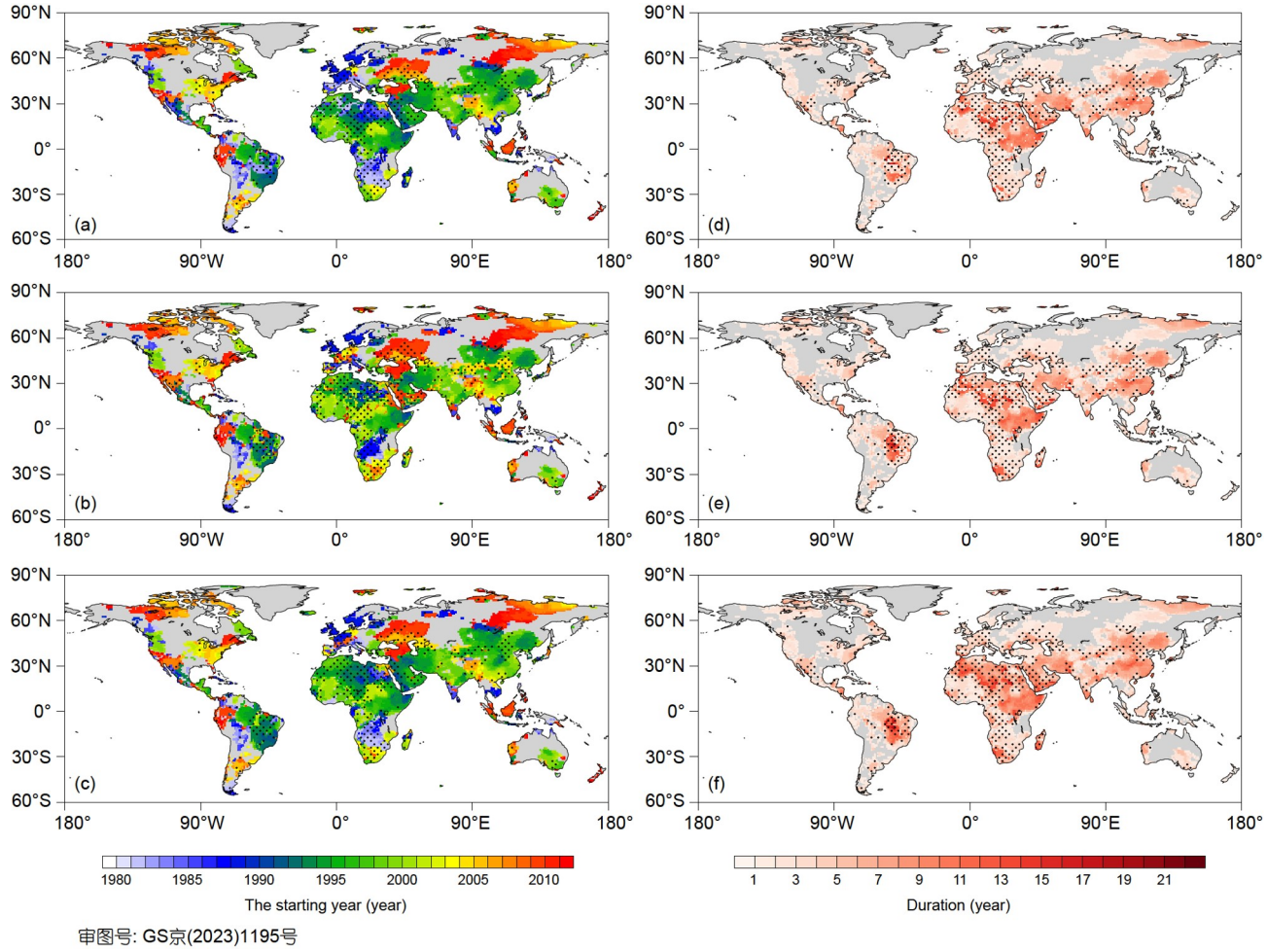

Figure 4 The starting years ((a)–(c)) and durations ((d)–(f)) of different persistent IDACs. (a), (d) The first persistent IDAC; (b), (e) the second persistent IDAC; and (c), (f) the persistent IDAC with the longest duration. If a grid point has only one persistent IDAC in the whole time series, the same IDAC is shown under the three selection conditions in the figure. The dotted regions show the areas in which two or more persistent IDACs occurred.

a significant VPD increase after 2005; this should be considered in subsequent climate studies to determine whether new significant atmospheric aridity stress and significant changes in the climate background field are occurring in this area. These persistent IDACs that have begun in the 21st century may be affected by increased temperature and warming and wetting in the high latitudes of the Northern Hemisphere (Zhu et al., 2016).

In preliminary VPD analyses, researchers have often used a fixed year as the criterion for dividing the period in some previous studies; such a selection has little impact on global-scale studies but has shortcomings for regional-scale studies; for example, IDACs that occurred late would be masked in some areas due to the use of this method. Four regions were selected in this paper based on the occurrence times of the persistent DAC, the duration, the starting year, and the key regions of land-atmosphere coupling proposed in previous studies (Qiao et al., 2022). These regions are shown in Figure 5a and correspond to eastern North America, western South America, central Africa, and high-latitude Asia; we found that the DAC information contained in the global time series cannot fully represent the changes in some individual regions. The fixed year (1994) in these regions is not the year in which the VPD began to change significantly, and the following points need to be noted: (1) some stages with opposite VPD changes may be difficult to fully perform due to the segmentation of the time series, for example, there are two DACs lasted 1 year in eastern North America after 1980, which are the DDAC in 1992 and the IDAC in 2005, and considering a fixed year would make the DDAC challenging to show (Figure 5b); (2) for significant increases that occurred relatively early or late, the trends obtained for the periods before and after the fixed year deviated from the actual situation, for example, the three IDACs identified in central Africa after 1980 occurred in 1983, 1987, and 2001, and it can be clearly observed that central Africa showed a significant increase in the early 1980s, while the persistent IDAC occurred in high-latitude Asia after 1980 was from 2009 to 2011, and the obvious increasing trend in the VPD in high latitudes after 2005 would be weakened by setting an

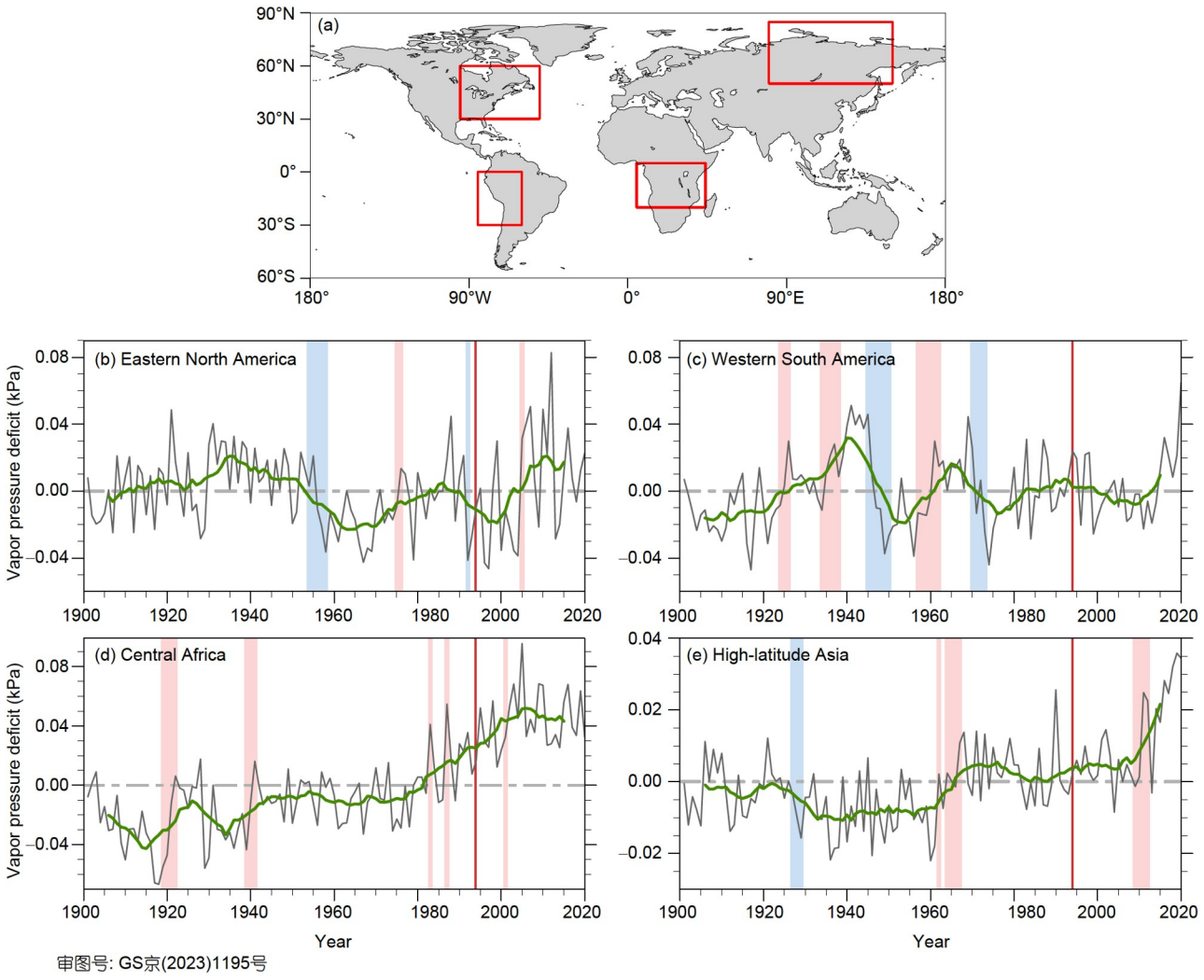

Figure 5 The characteristics of VPD changes in selected regions. (a) Selected regions for analysis; (b) eastern North America (30°–60°N, 50°–95°W); (c) western South America (0°–30°S, 60°–85°W); (d) central Africa (20°S–5°N, 5°–44°E); and (e) high-latitude Asia (50°–85°N, 80°–150°E). The black solid line is the time series of the regional annual average of the monthly VPD anomalies, the green solid line is the 11-year running mean of the regional average VPD anomalies, the red shadow is the persistent IDAC, the blue shadow is the persistent DDAC, and the red vertical line is the starting year (1994) in which the persistent global land average VPD IDAC occurred after 1980.

early cutting point (Figure 5d, e); and (3) the fluctuations in some areas, such as western South America, would be masked to some extent (Figure 5c).

Our analysis of the selected areas does not negate the conclusions obtained from the segmentation of the global average VPD in previous studies, and there is consensus regarding the roles of the VPD in vegetation and ecosystem carbon fluxes at the global scale among the results obtained by many researchers (Novick et al., 2016; Yuan et al., 2019; Grossiord et al., 2020; He et al., 2022). Our study focuses more on illustrating that for regional-scale research objects, and more information should be combined to select the cutting point for the corresponding analysis. For example, when studying VPD changes at a regional scale, one can first focus on the spatial distributions of the occurrence times and the starting year of persistent IDACs and persistent DDACs at the global scale to understand the occurrence time and spatial range of significant decadal VPD changes, and then analyse target areas based on this information to determine the cutting point at which significant changes occurred by the starting year, so as to analyse the complex situation caused by regional differences in greater detail.

3.3 Possible causes of the persistent IDAC of the VPD

The possible causes of the significant VPD changes identified in the longest-duration persistent IDAC phase were analysed by multiple linear regression from the two influencing factors of the actual vapor pressure and temperature. The VPD was positively correlated with temperature during the historical period (1901–2020), especially in low latitudes, such as Africa and South America, where each 1 °C increase in temperature was accompanied by a VPD increase of more than 0.2 kPa (Figure 6a); while the VPD was ne-

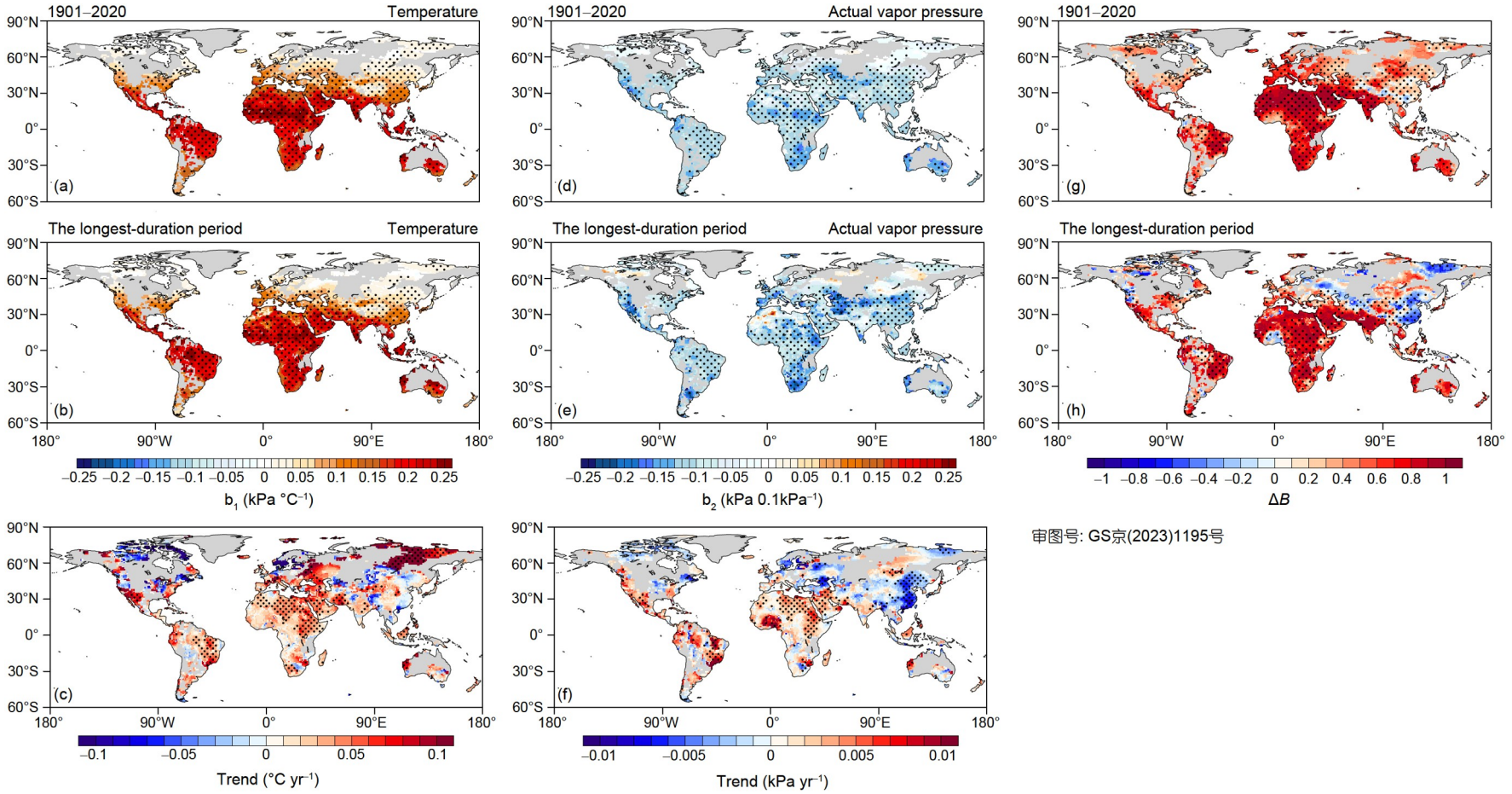

审图号: GS京(2023)1195号

Figure 6 Multiple linear regression and trend results. (a), (d) The partial regression coefficients of the VPD with the temperature and actual vapor pressure for 1901–2020; (b), (e) the partial regression coefficients of the VPD with the temperature and actual vapor pressure in the longest-duration persistent IDAC period; (c), (f) temperature and actual vapor pressure trends in the longest-duration persistent IDAC period; (g), (h) the relative influences of the temperature and actual vapor pressure on the VPD from 1901 to 2020 and during the longest-duration persistent IDAC period. In (g) and (h), ΔB is the difference between the absolute value of the standardized partial regression coefficient of the temperature ($B1$) and the absolute value of the standardized partial regression coefficient of the actual vapor pressure ($B2$); this term is calculated as $\Delta B=|B1|-|B2|$; see Methods 2.2.2 for details. Panels (a) and (b) denote the VPD change per 1 °C temperature change (kPa °C^{-1}); panels (d) and (e) denote the VPD change per 0.1 kPa actual vapor pressure change (kPa 0.1 kPa^{-1}); the time range of the period in panels (b) and (e) is from the first year of the persistent IDAC to the tenth year after the last year of the persistent IDAC. The black dotted area is the area that passed the 95% significance test.

gatively correlated with the actual vapor pressure on a global scale, with each 0.1 kPa decrease in the actual vapor pressure causing a VPD increase of more than 0.05 kPa in most parts of the world (Figure 6d). In the period of the longest-duration persistent IDAC, the VPD was still significantly positively correlated with the temperature, but in most parts of China and Central Asia, the VPD change caused by the actual vapor pressure increased significantly. For example, every 0.1 kPa decrease in the actual vapor pressure was accompanied by a VPD increase of approximately 0.15 kPa in northern China (Figure 6e). In addition, the effects of the temperature and actual vapor pressure on VPD were compared using the standardized partial regression coefficients in the two periods (Figure 6g, 6h, reference method 2.2.2). The effect of the temperature on the VPD was greater than the effect of the actual vapor pressure on the VPD in most areas during the historical period; while the effect of the actual vapor pressure on the VPD was greatly enhanced and even exceeded the effect of the temperature in most of China, Central Asia, northern Eastern Europe, and northern Central Siberia during the persistent IDAC period, although the VPD response to increasing temperature was still high at low latitudes. In general, the VPD exhibited a high response to the temperature at low latitudes during both the historical and the persistent IDAC period, but the effect of the actual vapor pressure was greatly enhanced during the persistent IDAC period in some places, such as middle latitude Asia.

Combining the trend changes of the temperature and actual vapor pressure (Figure 6c, 6f), it can be found that the temperature had a greater influence on the VPD in low latitudes (Figure 6h), although both the temperature and actual vapor pressure were increasing, especially in Africa and South America, so the increase of temperature was the main reason for the persistent IDAC of VPD in these regions; the temperature increase was accompanied by a decrease in the actual vapor pressure in some other regions, such as western Eastern Europe, western China and northern Central Siberia, where the temperature increase and actual vapor pressure decrease combined to cause the persistent IDAC of the VPD; while the response of the VPD to the actual vapor pressure was greatly enhanced in the persistent IDAC period in eastern and northern China in the 1990s, and the persistent IDAC of VPD was caused mostly by the actual vapor pressure decrease. The strengthening of the water limitation may have been an essential factor in the persistent abrupt VPD increase observed in most parts of China, northern Eastern Europe, Central Asia, and other regions; while the significant VPD changes were more affected by global warming in other regions. In addition, the water limitation was strengthened in some areas where the starting year around 2010 (Figure 4c), so whether a change in soil moisture will exacerbate the atmospheric humidity limitation on the VPD and cause more frequent and more intense atmospheric aridity in more areas in the near future is a matter of concern.

3.4 Spatial and temporal characteristics of the VPD DDAC

Although the VPD DACs in the global land area mainly in the form of VPD increases, persistent DDACs also occurred in some areas, such as in central North America and around the Great Lakes, in the subtropical region of western South America, in central Africa and in parts of middle latitude Asia; however, these events were much smaller in number and duration, and the starting year is also significantly different (Figure 7). Although most of the regions with multiple persistent IDACs do not overlap with regions with persistent DDACs, significant decreases were still detected in some regions with multiple significant increases, such as central Africa and parts of Siberia, and attention should be given to the possible complexity of the climate background field and the model simulation accuracy in these regions. In addition, the abnormal VPD decreases observed in Africa and parts of Asia in the last decade are also worthy of attention under global warming and intensified atmospheric aridity. It should be noted that if both an IDAC and a DDAC occurred in a certain period, the positive (negative) VPD trend might conceal the DDAC (IDAC). For example, in north-eastern China, the VPD trend after 1994 was smaller than that before 1994 (Figure 7a), but there was a long-lasting persistent IDAC around 1995 (Figure 4c); this decreasing trend also obscured the significant VPD increase that occurred in northern North America after 2005 (Figure 4c), which may have led to the rapid development of atmospheric aridity in the short term and posed challenges to ecology and human society; in addition, the trend after 1994 increased compared to those before 1994 in western North America and parts of central Africa, but a significant persistent DDAC continued after 1994.

4. Conclusion and discussion

In this paper, we analysed the spatial and temporal characteristics of the VPD DACs that occurred globally over a period of more than one hundred years with CRU data and statistical analysis methods such as the moving t test; we focused on the situation after 1980. The results show that the persistent IDAC occurrence times of VPD from 1980 to 2020 mainly presented a spatial distribution of more occurrences in the middle and low latitudes and fewer occurrences in the high latitudes, with most regions experiencing fewer than two persistent IDACs. Significantly more persistent IDACs were initiated between 1993 and 2001 than in other periods, and a large increase was again observed in 2009. The longest duration can be up to 22 years, with significantly longer

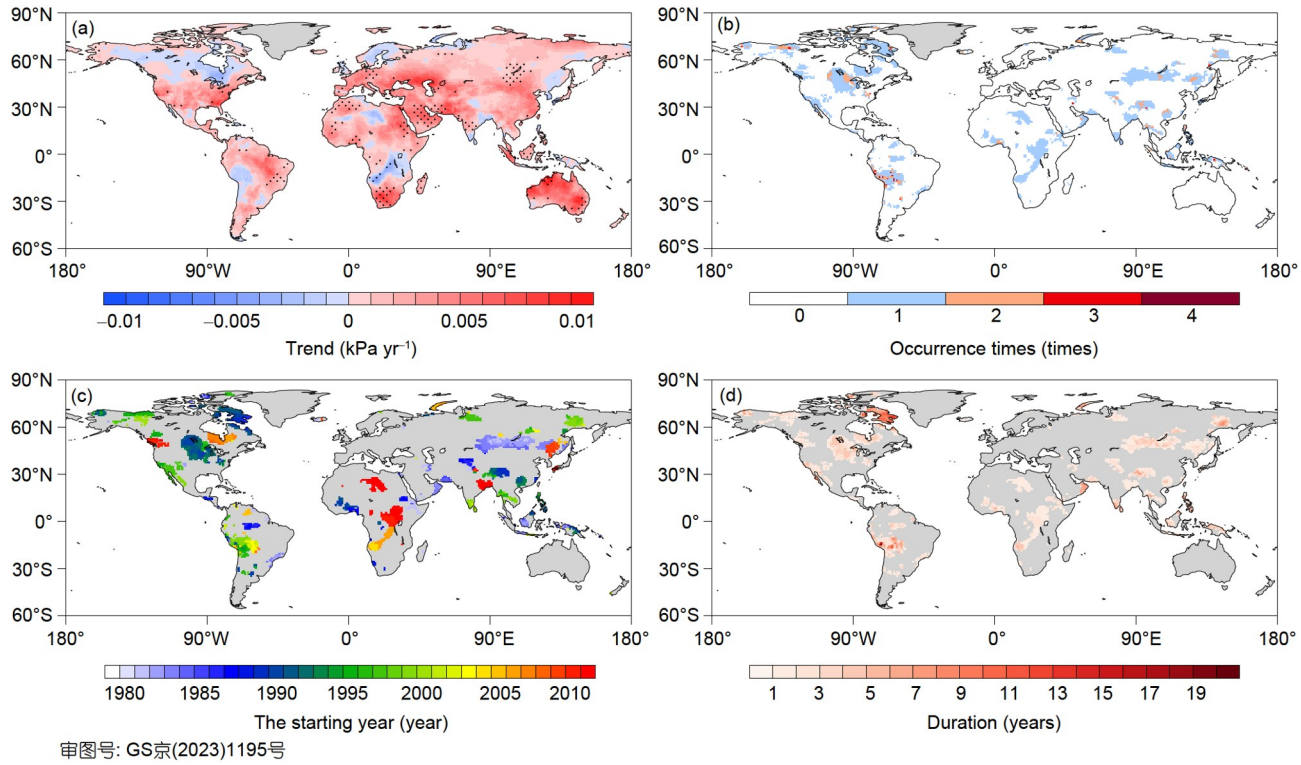

Figure 7 Spatial distribution of persistent DDACs. (a) The trend difference before and after 1994; (b) the persistent DDAC occurrence times at the global scale; (c) the starting year of the longest-duration persistent DDAC. The dotted area in panel (a) passed the 95% significance test in both the periods before and after 1994.

durations observed in the 1990s than in other periods. The increased number and duration of persistent IDACs together caused a rapid expansion of regions with significantly increased VPD in the 1990s and in approximately 2010. The starting years of persistent IDACs were early in the middle and low latitudes and late in the high latitudes, and the durations were significantly longer in the middle and low latitudes, indicating that atmospheric aridity intensified first in the middle and low latitudes. For the period of the persistent IDAC with the longest duration, the water limitation on the VPD was significantly enhanced in Central Asia and most parts of China. In addition, there were some regions with persistent DDACs, but the range, occurrence frequency and duration of the persistent DDAC were significantly less than those of a persistent IDAC.

The study conducted in this paper suggests that the selection of the regional turning year is important when studying the regional VPD or atmospheric aridity. The VPD is generally affected by a number of factors comprehensively, as has been shown in some past studies: an increase in temperature directly leads to an increase in the saturated vapor pressure, which further contributes to an increase in the VPD when the surface relative humidity changes little (Allen et al., 1998; Williams et al., 2013); a decrease in ocean evaporation is an important mechanism responsible for decreased actual vapor pressure on land (Stocker et al., 2014; Fu and Feng, 2014; Yuan et al., 2019); in addition, a soil moisture decrease is another important reason for a decrease in land moisture and the moisture limitation resulting from the soil moisture to be further enhanced (Jung et al., 2010; Yuan et al., 2021; Denissen et al., 2022). The occurrence time, degree, and range of significant VPD changes differ due to large differences in the climate background field and changes in climate variables among different regions. The instability of climate change and the possible strong instability drivers should be considered in regions with multiple persistent DACs, especially in areas that have experienced transitions between the IDAC and DDAC.

In this study, we focused on significant persistent IDACs of the VPD that have occurred since 1980 and provided a preliminary analysis of the possible causes of the persistent IDAC with the longest duration. Global warming may be the main reason for the abrupt VPD increases experienced in regions such as Africa and South America in the 1990s, but enhanced water limitation may be the main reason for the rapid development of the VPD in the high latitudes of the Northern Hemisphere and in parts of Europe over the last decade, and the negative feedback effect between the VPD and soil moisture may also plays an important role (Zhou et al., 2019a; Konapala et al., 2020; Zhou et al., 2021; Barkhordarian et al., 2021). The forcing effect of aerosols may also be another factor affecting the VPD IDACs over the past

10 years (Barkhordarian et al., 2019), and therefore, the persistent IDAC of VPD and its causes over the last 10 years deserve more in-depth investigation. At the same time, some scientific questions that deserve close attention under the background of global surface temperature are raised (Zuo et al., 2021): will the VPD again experience a large-scale significant IDAC? Will the water limitation on the VPD be further strengthened in some regions? Will there be more frequent and more intense atmospheric aridity in more regions? And what are the respective roles of energy and water limitations, and will these factors significantly impact the regional climate and ecosystem? The land-atmosphere coupling process is not accurate in existing Earth system models, and the feedback mechanisms between the VPD and variables such as evapotranspiration, vegetation, and carbon flux remain to be improved (Yuan et al., 2019; Berg and McColl, 2021; Liu et al., 2021). The results and discussion in this paper can provide a reference for other researchers to isolate the effect of the VPD in the climate system (Zhou et al., 2019b), improve the response mechanisms to atmospheric aridity in models, and reduce the uncertainty of future projections (Grossiord et al., 2020; Humphrey et al., 2021).

The change of the mean value is the main reason for VPD DACs in most parts of the globe, and this should be pointed out in the content that the moving t test was used in this paper. The absolute mean value changes were small in only a few regions, such as the Qinghai-Tibet Plateau and the high latitudes of the Northern Hemisphere, but the large relative changes in these regions make them also worthy of attention. The contents of this work provide an idea for other researchers to use variance to study the significant changes caused by VPD fluctuations in the historical period, especially in areas with small mean changes. This study is helpful for deepening our understanding of the characteristics of VPD changes in the historical period, the development of atmospheric aridity and the possible impact mechanisms, and provides an important reference for solving the problems associated with atmospheric aridity and alleviating increasingly severe atmospheric aridity events.

Acknowledgements *This work was supported by the National Key Research and Development Program of China (Grant No. 2022YFF0801703) and the National Natural Science Foundation of China (Grant Nos. 42175053 & 41822503).*

References

Allen R G, Pereira L S, Raes D, Smith M. 1998. Crop evapotranspiration—Guidelines for computing crop water requirements—FAO Irrigation and drainage paper 56. Rome: Food and Agriculture Organization of the United Nations

Barkhordarian A, Bowman K W, Cressie N, Jewell J, Liu J. 2021. Emergent constraints on tropical atmospheric aridity-carbon feedbacks and the future of carbon sequestration. Environ Res Lett, 16: 114008

Barkhordarian A, Saatchi S S, Behrangi A, Loikith P C, Mechoso C R. 2019. A recent systematic increase in vapor pressure deficit over tropical South America. Sci Rep, 9: 15331

Berg A, McColl K A. 2021. No projected global drylands expansion under greenhouse warming. Nat Clim Chang, 11: 331–337

Denissen J M C, Teuling A J, Pitman A J, Koirala S, Migliavacca M, Li W, Reichstein M, Winkler A J, Zhan C, Orth R. 2022. Widespread shift from ecosystem energy to water limitation with climate change. Nat Clim Chang, 12: 677–684

Ficklin D L, Novick K A. 2017. Historic and projected changes in vapor pressure deficit suggest a continental-scale drying of the United States atmosphere. J Geophys Res-Atmos, 122: 2061–2079

Friedlingstein P, Jones M W, O′Sullivan M, Andrew R M, Bakker D C E, Hauck J, Le Quéré C, Peters G P, Peters W, Pongratz J, Sitch S, Canadell J G, Ciais P, Jackson R B, Alin S R, Anthoni P, Bates N R, Becker M, Bellouin N, Bopp L, Chau T T T, Chevallier F, Chini L P, Cronin M, Currie K I, Decharme B, Djeutchouang L M, Dou X, Evans W, Feely R A, Feng L, Gasser T, Gilfillan D, Gkritzalis T, Grassi G, Gregor L, Gruber N, Gürses Ö, Harris I, Houghton R A, Hurtt G C, Iida Y, Ilyina T, Luijkx I T, Jain A, Jones S D, Kato E, Kennedy D, Klein Goldewijk K, Knauer J, Korsbakken J I, Körtzinger A, Landschützer P, Lauvset S K, Lefèvre N, Lienert S, Liu J, Marland G, McGuire P C, Melton J R, Munro D R, Nabel J E M S, Nakaoka S I, Niwa Y, Ono T, Pierrot D, Poulter B, Rehder G, Resplandy L, Robertson E, Rödenbeck C, Rosan T M, Schwinger J, Schwingshackl C, Séférian R, Sutton A J, Sweeney C, Tanhua T, Tans P P, Tian H, Tilbrook B, Tubiello F, van der Werf G R, Vuichard N, Wada C, Wanninkhof R, Watson A J, Willis D, Wiltshire A J, Yuan W, Yue C, Yue X, Zaehle S, Zeng J. 2022. Global carbon budget 2021. Earth Syst Sci Data, 14: 1917–2005

Fu C B, Wang Q. 1992. The definition and detection of the abrupt climatic change (in Chinese). Chin J Atmos Sci, 16: 482–493

Fu Q, Feng S. 2014. Responses of terrestrial aridity to global warming. J Geophys Res-Atmos, 119: 7863–7875

Green J K, Berry J, Ciais P, Zhang Y, Gentine P. 2020. Amazon rainforest photosynthesis increases in response to atmospheric dryness. Sci Adv, 6: eabb7232

Grossiord C, Buckley T N, Cernusak L A, Novick K A, Poulter B, Siegwolf R T W, Sperry J S, McDowell N G. 2020. Plant responses to rising vapor pressure deficit. New Phytol, 226: 1550–1566

Harris I, Osborn T J, Jones P, Lister D. 2020. Version 4 of the CRU TS monthly high-resolution gridded multivariate climate dataset. Sci Data, 7: 109

He B, Chen C, Lin S, Yuan W, Chen H W, Chen D, Zhang Y, Guo L, Zhao X, Liu X, Piao S, Zhong Z, Wang R, Tang R. 2022. Worldwide impacts of atmospheric vapor pressure deficit on the interannual variability of terrestrial carbon sinks. Natl Sci Rev, 9: 8

Huang J Y. 2016. Statistical Analysis and Forecasting Methods in Meteorology (in Chinese). 4th ed. Beijing: China Meteorological Press

Humphrey V, Berg A, Ciais P, Gentine P, Jung M, Reichstein M, Seneviratne S I, Frankenberg C. 2021. Soil moisture-atmosphere feedback dominates land carbon uptake variability. Nature, 592: 65–69

Jung M, Reichstein M, Ciais P, Seneviratne S I, Sheffield J, Goulden M L, Bonan G, Cescatti A, Chen J, de Jeu R, Dolman A J, Eugster W, Gerten D, Gianelle D, Gobron N, Heinke J, Kimball J, Law B E, Montagnani L, Mu Q, Mueller B, Oleson K, Papale D, Richardson A D, Roupsard O, Running S, Tomelleri E, Viovy N, Weber U, Williams C, Wood E, Zaehle S, Zhang K. 2010. Recent decline in the global land evapotranspiration trend due to limited moisture supply. Nature, 467: 951–954

Konapala G, Mishra A K, Wada Y, Mann M E. 2020. Climate change will affect global water availability through compounding changes in seasonal precipitation and evaporation. Nat Commun, 11: 3044

Liu L, Gudmundsson L, Hauser M, Qin D, Li S, Seneviratne S I. 2020. Soil moisture dominates dryness stress on ecosystem production globally. Nat Commun, 11: 4892

Liu Y, Li Z, Chen Y. 2021. Continuous warming shift greening towards browning in the Southeast and Northwest High Mountain Asia. Sci Rep, 11: 17920

Lu H, Qin Z, Lin S, Chen X, Chen B, He B, Wei J, Yuan W. 2022. Large

influence of atmospheric vapor pressure deficit on ecosystem production efficiency. Nat Commun, 13: 1653
Novick K A, Ficklin D L, Stoy P C, Williams C A, Bohrer G, Oishi A C, Papuga S A, Blanken P D, Noormets A, Sulman B N, Scott R L, Wang L, Phillips R P. 2016. The increasing importance of atmospheric demand for ecosystem water and carbon fluxes. Nat Clim Change, 6: 1023–1027
Piao S, Wang X, Park T, Chen C, Lian X, He Y, Bjerke J W, Chen A, Ciais P, Tømmervik H, Nemani R R, Myneni R B. 2020. Characteristics, drivers and feedbacks of global greening. Nat Rev Earth Environ, 1: 14–27
Qiao L, Zuo Z, Xiao D. 2022. Evaluation of soil moisture in CMIP6 simulations. J Clim, 35: 779–800
Shi N. 2009. Meteorological Statistics and Forecasting (in Chinese). Beijing: China Meteorological Press
Song Y, Jiao W, Wang J, Wang L. 2022. Increased global vegetation productivity despite rising atmospheric dryness over the last two decades. Earths Future, 10: 16
Stocker T F, Qin D, Plattner G K, Tignor M M B, Allen S K, Boschung J, Nauels A, Xia Y, Bex V, Midgley P M. 2014. Climate Change 2013—The Physical Science Basis: Working Group I Contribution to the Fifth Assessment Report of the Intergovernmental Panel on Climate Change. Cambridge: Cambridge University Press
Toms J D, Lesperance M L. 2003. Piecewise regression: A tool for identifying ecological thresholds. Ecology, 84: 2034–2041
Wang J, Tong J L, Xiao Y Q, Wu X Y, Zhang W Y. 2018. Interdecadal variation characteristics of summer sensible heat flux in typical arid and semi-arid areas of East Asia (in Chinese). Arid Meteor, 36: 203–211
Wei F Y. 2007. Modern Climate Statistical Diagnosis and Prediction Techniques (in Chinese). 2nd ed. Beijing: China Meteorological Press
Williams A P, Allen C D, Macalady A K, Griffin D, Woodhouse C A, Meko D M, Swetnam T W, Rauscher S A, Seager R, Grissino-Mayer H D, Dean J S, Cook E R, Gangodagamage C, Cai M, McDowell N G. 2013. Temperature as a potent driver of regional forest drought stress and tree mortality. Nat Clim Change, 3: 292–297
Williams A P, Seager R, Macalady A K, Berkelhammer M, Crimmins M A, Swetnam T W, Trugman A T, Buenning N, Noone D, McDowell N G, Hryniw N, Mora C I, Rahn T. 2015. Correlations between components of the water balance and burned area reveal new insights for predicting forest fire area in the southwest United States. Int J Wildland Fire, 24: 14–26
Xiao D, Li J P. 2007. Main decadal abrupt changes and decadal modes in global sea surface temperature field (in Chinese). Chin J Atmos Sci, 31: 839–854
Yuan R R, Huang X L, Hao L. 2021. Spatiotemporal variation of vapor pressure deficit and impact factors in China in the past 40 years (in Chinese). Climatic Environ Res, 26: 413–424
Yuan W, Zheng Y, Piao S, Ciais P, Lombardozzi D, Wang Y, Ryu Y, Chen G, Dong W, Hu Z, Jain A K, Jiang C, Kato E, Li S, Lienert S, Liu S, Nabel J E M S, Qin Z, Quine T, Sitch S, Smith W K, Wang F, Wu C, Xiao Z, Yang S. 2019. Increased atmospheric vapor pressure deficit reduces global vegetation growth. Sci Adv, 5: eaax1396
Zeng Z, Piao S, Li L Z X, Zhou L, Ciais P, Wang T, Li Y, Lian X, Wood E F, Friedlingstein P, Mao J, Estes L D, Myneni R B, Peng S, Shi X, Seneviratne S I, Wang Y. 2017. Climate mitigation from vegetation biophysical feedbacks during the past three decades. Nat Clim Change, 7: 432–436
Zhou S, Williams A P, Berg A M, Cook B I, Zhang Y, Hagemann S, Lorenz R, Seneviratne S I, Gentine P. 2019a. Land-atmosphere feedbacks exacerbate concurrent soil drought and atmospheric aridity. Proc Natl Acad Sci USA, 116: 18848–18853
Zhou S, Williams A P, Lintner B R, Berg A M, Zhang Y, Keenan T F, Cook B I, Hagemann S, Seneviratne S I, Gentine P. 2021. Soil moisture-atmosphere feedbacks mitigate declining water availability in drylands. Nat Clim Chang, 11: 38–44
Zhou S, Zhang Y, Park Williams A, Gentine P. 2019b. Projected increases in intensity, frequency, and terrestrial carbon costs of compound drought and aridity events. Sci Adv, 5: eaau5740
Zhu Z, Piao S, Myneni R B, Huang M, Zeng Z, Canadell J G, Ciais P, Sitch S, Friedlingstein P, Arneth A, Cao C, Cheng L, Kato E, Koven C, Li Y, Lian X, Liu Y, Liu R, Mao J, Pan Y, Peng S, Peñuelas J, Poulter B, Pugh T A M, Stocker B D, Viovy N, Wang X, Wang Y, Xiao Z, Yang H, Zaehle S, Zeng N. 2016. Greening of the Earth and its drivers. Nat Clim Change, 6: 791–795
Zuo Z, Xiao D, He Q. 2021. Role of the warming trend in global land surface air temperature variations. Sci China Earth Sci, 64: 866–871

(Responsible editor: Zhaoxin LI)